atmosphere

MDPI

Article

Kinetic Studies on the Steam Gasification of Chars Derived from Coals by Different Isoconversional Methods

Mei An [1,*] and Qingjie Guo [2,*]

[1] Key Laboratory of Coal Processing and Efficient Utilization, China University of Mining & Technology, Xuzhou 221116, China
[2] State Key Laboratory of High-Efficiency Coal Utilization and Green Chemical Engineering, School of Chemistry and Chemical Engineering, Ningxia University, Yinchuan 750021, China
* Correspondence: anmei_712@163.com (M.A.); qjguo@qust.edu.cn (Q.G.)

Abstract: Previous studies have successfully assessed the extent to which a kinetic model accurately represents a specific reaction mechanism by comparing the kinetic parameters derived from the kinetic model to those obtained using isoconversional methods. However, this approach remains underdeveloped for the important steam gasification reaction of char. This study addresses this issue by conducting a series of steam-assisted char gasification tests, using thermogravimetric analysis at five different heating rates. The results indicate that the carbon conversion ratio of the char gasification reaction increases with the increasing heating rate. The activation energies of the reaction process are determined with different carbon conversion ratios using three isoconversional methods, including the Flynn–Wall–Ozawa, Kissinger–Akahira–Sunose, and Starink methods. The gasification mechanism is also analyzed using model-fitting methods with a wide variety of carbon conversion models, and the accuracies of the models are evaluated, firstly, by comparing the obtained goodness of fit values of the models with the experimental results, and, secondly, by comparing the obtained activation energies with those derived using the isoconversional methods. The goodness of fit results and the results of the comparisons between the activation energies obtained using the various models with the isoconversional values demonstrate that the three-dimensional Avrami–Erofeev model best represents the steam gasification char reaction, where the difference between the two activation energy values is only 0.70 KJ.mol^{-1}. The reliability of the proposed approach for evaluating the applicability of a given kinetic model to the steam gasification reaction of char is tested by comparing the results obtained for char samples derived from three different bituminous coal sources.

Keywords: steam gasification; activation energy; kinetic model; isoconversional method; model-fitting method

check for updates

Citation: An, M.; Guo, Q. Kinetic Studies on the Steam Gasification of Chars Derived from Coals by Different Isoconversional Methods. *Atmosphere* **2022**, *13*, 1480. https://doi.org/10.3390/atmos13091480

Academic Editor: Yoshizumi Kajii

Received: 26 July 2022
Accepted: 6 September 2022
Published: 12 September 2022

Publisher's Note: MDPI stays neutral with regard to jurisdictional claims in published maps and institutional affiliations.

Copyright: © 2022 by the authors. Licensee MDPI, Basel, Switzerland. This article is an open access article distributed under the terms and conditions of the Creative Commons Attribution (CC BY) license (https://creativecommons.org/licenses/by/4.0/).

1. Introduction

Coal gasification is a well-developed means of converting coal into a clean energy source for heating and electricity generation purposes and for the production of chemical feedstocks. Typically, coal gasification is a two-step process, involving reactions that are categorized into pyrolysis, gasification, and gas-phase reaction mechanisms. The first stage, the pyrolysis process, generates vaporous components by heating the coal at a relatively low temperature (450–600 °C) in the absence of air. The separation of these vaporous components leaves behind a residue of charcoal, which is converted, in a second stage, the char gasification process, into carbon monoxide (CO) through reactions with oxygen-bearing compounds at a relatively high temperature (700–1200 °C). Clearly, char gasification represents the rate-limiting step of the coal gasification process, and numerous methods have been developed for analyzing the reaction kinetics of char gasification [1–3] in an effort to enhance the gasification rate at lower temperatures, which is crucial for supporting efficient coal gasification applications. These analytical methods can be divided

into two categories, including model-fitting methods and model-free, or isoconversional, methods. [4–6].

The model-fitting method has been frequently used because it facilitates the direct analysis of reaction kinetics [7,8]. Complex models can be developed with a large number of kinetic parameters that lead to data with an improved fit with the experimental results, where the goodness of fit is generally assessed based on calculations of the coefficient of determination (R^2). However, while these models may fit better with the experimental data, the kinetic parameters obtained through fitting can be inconsistent, and thereby lead to incorrect assessments of the reaction mechanism. Hence, an indication of good model fitting, such as high R^2 values, alone is no longer considered as a valid basis for choosing the best reaction kinetics model [9].

The above-discussed shortcomings of model-fitting methods have led to the increased use of model-free methods, which require no assumptions regarding the char gasification reaction process when determining the kinetic parameters. However, this absence of model assumptions renders these methods incapable of facilitating a detailed analysis of the reaction mechanisms. As such, only the kinetic parameter values themselves are of substantial benefit.

The respective shortcomings of model-fitting and model-free methods have led researchers to develop new criteria for determining whether a given kinetic model adequately represents a specific reaction mechanism by comparing the kinetic parameters derived using a kinetic model with those obtained using model-free approaches [10,11]. For example, Czerski et al. [12] compared the kinetic parameters calculated using two first-order models and a combination of the model-free isoconversional method and model-dependent Coats–Redfern method in order to investigate the impact of direct and indirect char gasification processes conducted in CO_2 atmospheres on the activation energy of the reactions. Khaled O. Sebakhy et al. [13] studied the transformation of cubic molybdenum carbide into hexagonal β-Mo_2C through an Avrami–Erofeev kinetic model. Other studies have also focused on the kinetic parameters of char gasification reactions in CO_2 atmospheres [14,15]. However, research focusing on the evaluation of the kinetic parameters of the steam gasification of char is lacking.

In the present study, we addressed the above-mentioned issue by conducting a series of steam gasification tests for three types of bituminous chars using thermogravimetry analysis (TGA) and derivative thermogravimetry (DTG). The activation energy (E_a) of the steam gasification reaction of char was evaluated based on the experimental results, using three isoconversional methods, including the Flynn–Wall–Ozawa (FWO), Kissinger–Akahira-Sunose (KAS), and Starink methods, and it was also evaluated independently using a wide variety of kinetic models. The goodness of fit of these kinetic models (i.e., R^2 values) was applied as the first criterion for selecting the candidate models best representing the steam gasification reaction process. Then, the difference between the E_a values obtained using the model-free and those obtained using the model-fitting methods was examined as the second criterion for selecting the best possible kinetic model for this reaction process. The reliability of the proposed approach for the evaluation of the applicability of a given kinetic model to the steam gasification reaction of char was tested by comparing the results obtained for char samples derived from three different bituminous coal sources.

2. Experiments and Theory

2.1. Coal Samples and Char Preparation

Coal samples were collected from the Ningdong (NX), Shaanxi (SX), and Xinjiang (XJ) coalfields in western China, which can be seen in Figure S1. The main reasons for choosing these three places were their abundant coal reserves, distinctive characteristics, and energy bases. The nature of the coal differed. The XRD and SEM-EDS of the NX, SX, and XJ coal can be seen in Figures S2 and S3. The $CuFe_2O_4$ oxygen carriers were characterized using a Japanese MiniFlex 600 X-ray diffraction (XRD) instrument with a tube current and voltage of 15 mA and 40 kV, respectively. The morphology of the

sample was established using a JEOL JSM-7900F scanning electron microscopy (SEM) instrument (JEOL Ltd., Tokyo, Japan). The inorganic constituents mass fraction in coal was analyzed by an X diffraction fluorescence (XRF), as shown in Table S1. The heavy metal content of the initial coal samples was determined using ICP methods, which can be seen Table S2. Measurements were conducted using an Agilent 7000 ICP-OES instrument. The sample preparation process can be seen in the Supplementary Information, Section S3. According to the solid waste identification standard GB 34330-2017 and the hazardous waste identification standard for immersion toxicity, standard GB 5085.3-2007, the samples were judged to be non-hazardous substances before and after coal gasification.

The char was prepared from coal placed in a packed column in an inert atmosphere with a continuous nitrogen flow. It was heated at a rate of 10 K·min^{-1} up to 850 °C, which was maintained for 60 min so as to achieve full devolatilization. The generated chars had a mean particle size of 75–150 μm. The detailed proximate and ultimate analyses of the coal samples and their major ash constituents are listed in Table 1.

Table 1. Proximate and ultimate analyses of the coal samples.

	Proximate Analysis (w%)				**Ultimate Analysis (w%)**				
	Moisture	**Ash**	**Volatile**	**Fixed C**	**C**	**H**	**N**	**S**	**O**
NX	10.14	5.40	27.03	67.57	79.18	4.40	1.50	0.60	9.00
SX	15.40	3.88	32.37	65.00	76.06	3.50	0.29	0.44	15.83
XJ	6.88	5.07	29.26	67.15	65.33	4.989	0.75	0.14	24.02

2.2. Steam Gasification

The steam gasification of the char samples was conducted in atmospheric pressure using a thermogravimetric analyzer (NETZSCH STA 449F3, Eltmann, Germany). During gasification, 10 mg of a given char sample was placed in an alumina (Al_2O_3) crucible with a 12 mm internal diameter and heated from 373 K to 1173 K at five different rates of 4, 8, 12, 16, and 20 K·min^{-1}, while gaseous H_2O with a partial pressure of 50% and the remaining partial pressure adjusted by argon (Ar) was introduced at a flow rate of 200 mL/min. The weight loss of the sample was not maintained for 30 min so as to ensure complete gasification. To avoid inter-particle diffusion and intra-pore diffusion, we used a sample particle size of 100 μm [16,17].

2.3. Kinetics Analysis

2.3.1. Activation Energy Calculation

The degree of conversion (X) obtained at any point in time t during the char gasification reaction process:

$$X = \frac{w_0 - w_t}{w_0 - w_\infty} \tag{1}$$

where w_0 is the initial char sample weight (i.e., 10 mg), w_t is the char sample weight at time t (mg), and w_∞ is the final char sample weight (mg). This variable, along with E_a, the heating rate β (K·min^{-1}), the gas constant R = 8.314462 J·K^{-1}·mol^{-1}, and temperature T, represent the core variables employed when using the FWO, KAS, and Starink methods, each of which produces a straight line with a slope of E_a. These straight lines were plotted and fitted based on the appropriate pairs of data points obtained for 5 values of X in the range of 0.1–0.9 at each of the five heating rates.

The FWO method establishes the following relationship:

$$\ln \beta = \ln\left(\frac{AE_a}{RG(X)}\right) - 5.3305 - 1.052\left(\frac{E_a}{RT}\right) \tag{2}$$

where A is the rate constant of the reaction (min^{-1}) and $G(X)$ is an integral function, which is defined in the following subsection. Here, the associated fitting is conducted based on the $\ln\beta$ and $1000/T$ data point pairs. The KAS method establishes the following relationship:

$$\ln\left(\frac{\beta}{T^2}\right) = \ln\left(\frac{AR}{E_a G(X)}\right) - \frac{E_a}{RT} \quad (3)$$

Here, the associated fitting is conducted based on the $\ln(\beta/T^2)$ and $1000/T$ data point pairs. The Starink method establishes the following relationship:

$$\ln\left(\frac{\beta}{T^{1.92}}\right) = -1.008\left(\frac{E_a}{RT}\right) + const \quad (4)$$

Here, the associated fitting is conducted based on the $\ln(\beta/T^{1.92})$ and $1000/T$ data point pairs.

2.3.2. Kinetic Model Analysis Methodology

According to Equations (2)–(4), the value of E_a, as the slope of the plotted lines, is unaffected by any of the terms in the given intercepts of the relationships. As such, E_a is independent of the reaction mechanism, while all the terms reflecting the reaction mechanism itself are contained within the intercepts. The kinetic model, reflecting the reaction mechanism, was determined using the methodology established by the ICTAC Kinetics Committee [18], and this method was employed to calculate $G(X)$ [19]:

$$\ln[G(X)] = \ln\left(\frac{AE_a}{R\beta}\right) - 2.315 - 0.4567\frac{E_a}{RT} \quad (5)$$

This represents a model-fitting approach for determining E_a based on the slope of a linear plot of $\ln[G(X)]$ versus $1000/T$, obtained using a series of common candidate $G(X)$ functions, including the power law (X^α), first-order Mampel ($-\ln(1-X)$), Avrami–Erofeev ($[-\ln(1-X)]^\alpha$), contracting sphere ($1-(1-X)^\alpha$), one-dimensional (1D) diffusion (X^2), two-dimensional (2D) diffusion ($(1-X)\ln(1-X)+X$), and three-dimensional (3D) diffusion $1-(1-X)^{1/3}$ or $1-2/3X-(1-X)^{3/2}$) functions, where various exponent values of α are employed, such as $1/4$, $1/3$, $1/2$, and $3/2$. The R^2 values obtained from the fitting results with the various candidate functions $G(X)$ can then be employed in order to determine the best-fitting model for describing the reaction process. If several linear relations between $\ln[G(X)]$ and $1000/T$ were obtained, the model with the smallest difference between the E_a values obtained from the specific kinetic model and the model-free isoconversional methods was chosen as the best-fitting model.

2.3.3. Pre-Exponential Factor Calculation

The pre-exponential factor A was determined using the intercept of Equation (5) for the best-fitting kinetic model, obtained according to the methodology discussed in the preceding subsection [20].

3. Results and Discussion

3.1. Effect of the Heating Rate on the Char Conversion

The TGA and DTG results obtained for the char sample derived from the NX coal source during steam gasification at different values of β are presented in Figure 1, and the characteristic parameters of the gasification processes, including the temperature, corresponding to the weight loss peak (T_{max}), the ultimate weight loss during char gasification (M_r), and the maximum rate of the weight loss (R_{max}), are listed in Table 2. The results demonstrate that the heating rate had obvious positive effects on the rate of the carbon conversion. Here, the value of T_{max} increased from 850 °C to 908 °C as β increased from 4 to 20 K·min^{-1}. We also noted that the value of R_{max} correspondingly increased from

3.48 to 15.69 wt%·min^{-1}. However, the value of M_r increased only slightly with increasing β. These findings reveal that increasing heating rates led to increasingly rapid reaction processes with short reaction times, but it did not alter the reaction mechanism itself. Specifically, the values of the weight loss of the char in the steam atmosphere were relatively similar at different heating rates, while the value of X increased with increasing β. Therefore, increased values of R_{max} were attained by increasing β. Nevertheless, the transfer of thermal energy from the external environment to the particle interiors is impeded at high heating rates, which is expected to result in a large temperature gradient within the particles. Consequently, this leads to thermal hysteresis patterns, and the value of T_{max} tends to shift toward higher temperatures at higher heating rates.

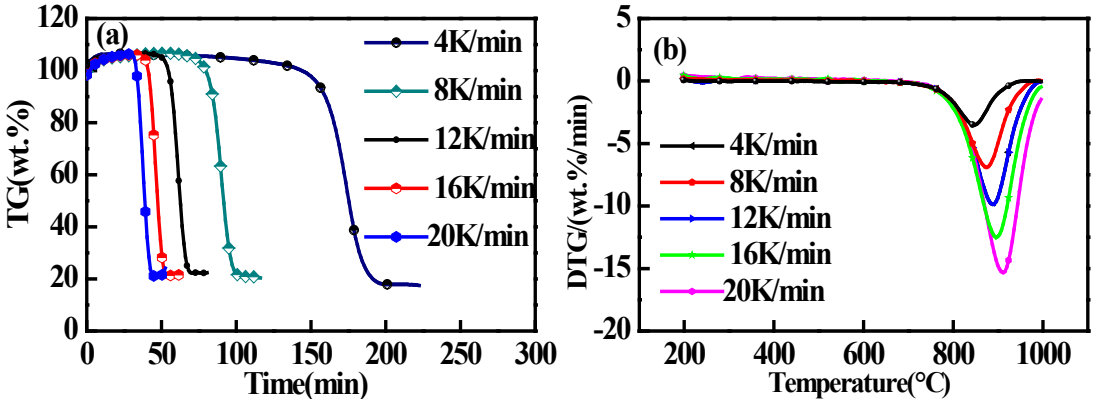


Figure 1. Thermal analyses of the gasification of the char sample derived from the NX coal source at different heating rates: (**a**) TGA; (**b**) DTG.

Table 2. Characteristic parameters of the steam gasification of char derived from Figure 1 at different heating rates β. The parameters include the temperature, corresponding to the weight loss peak (T_{max}), the ultimate weight loss during char gasification (M_r), and the maximum rate of weight loss (R_{max}).

β (K·min^{-1})	T_{max} (°C)	M_r (wt%)	R_{max} (wt%·min^{-1})
20	908	23.05	15.69
16	900	22.81	12.71
12	889	22.71	9.95
8	872	22.47	7.00
4	850	22.46	3.48

3.2. Activation Energy Values Obtained Using Isoconversional Methods

The plots and fitted lines obtained from the TGA data in Figure 1, which are based on the three isoconversional methods at the carbon conversion ratios X in the range of 0.1–0.9, are presented in Figure 2. In addition, the E_a values and corresponding values of R^2 obtained from the fitting results are listed in Table 3 for each value of X. We note that the values of R^2 obtained using all three methods were generally greater than 0.9. In addition, the values of E_a nearly always increased monotonically with increasing X. From the initially low values of E_a at $X = 0.1$, the values of E_a increased more slowly from 135.28 to 176.19 KJ.mol^{-1} (FWO), 114.74 to 152.13 KJ.mol^{-1} (KAS), and 115.39 to 152.87 KJ.mol^{-1} (Starink) with increasing X in the range of 0.2–0.9.The relatively low values of E_a obtained at $X = 0.1$ may be attributable to changes in the surfaces of the char particles in this early stage of gasification, affecting various factors such as the gas adsorption behavior of the active components, mineral catalysis [21,22], and pore structure [23]. In addition, we note from the average values of E_a (E_{ave}) derived from the FWO, KAS, and Starink methods for $0.2 \leq X \leq 0.8$ that the value of E_{ave} obtained using the FWO method is somewhat greater than those obtained using the KAS and Starink methods, while the values of E_{ave} obtained using the KAS and Starink methods are in good agreement and differ by less than 0.1%,

indicating that these E_{ave} values have a high degree of confidence. Therefore, we employed the E_{ave} value obtained using the Starink method ($E_{Starink}$) as the standard value for the comparison with the E_{ave} values obtained using the kinetic models.

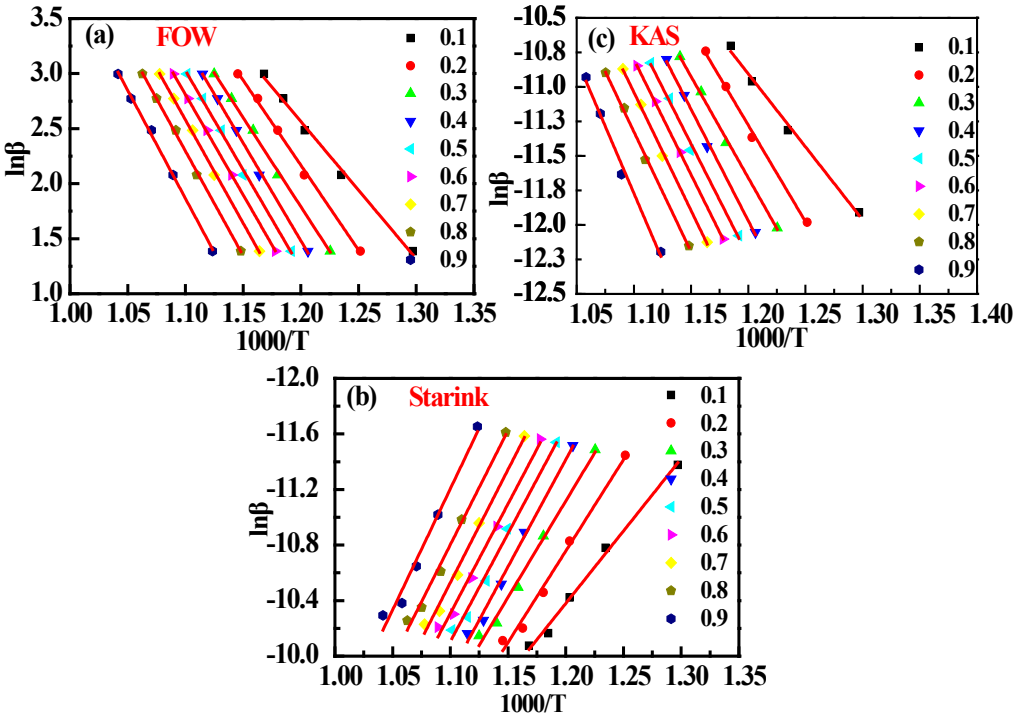


Figure 2. Plots of the isoconversional methods for the carbon conversion ratios X in the range of 0.1–0.9: (**a**) FWO method (Equation (2)); (**b**) KAS method (Equation (3)); (**c**) Starink method (Equation (4)).

Table 3. Activation energies E_a (KJ.mol^{-1}) of the steam gasification reaction of the char obtained at different values of X using the FWO, KAS, and Starink methods. The average value of E_a (E_{ave}) obtained for $0.2 \leq X \leq 0.8$ is also presented.

Degree of Conversion (X)	FOW Method		KAS Method		Starink Method	
	E_a	R^2	E_a	R^2	E_a	R^2
0.1	109.54	0.9948	90.66	0.9918	91.27	0.9933
0.2	135.28	0.9974	114.74	0.9959	115.39	0.9861
0.3	144.96	0.9982	123.66	0.9978	124.33	0.9881
0.4	158.07	0.9981	135.94	0.9961	136.62	0.9899
0.5	159.94	0.9974	137.54	0.9933	138.23	0.9880
0.6	159.44	0.9998	140.89	0.9999	141.59	0.9901
0.7	166.98	0.9986	143.90	0.9970	144.61	0.9896
0.8	169.07	0.9984	145.69	0.9972	146.40	0.9887
0.9	176.19	0.9978	152.13	0.9888	152.87	0.9743
E_{ave}	156.25 ± 20		134.62 ± 20		135.31 ± 20	

3.3. Analysis of Kinetic Models

The values of R^2 obtained by fitting the results to $\ln[G(X)]$ with respect to $1000/T$ in Equation (5) for $0.2 < X \leq 0.8$ at various heating rates and integral functions $G(X)$ are listed in Table 4. The results indicate that all the models considered provided gradually decreasing values of R^2 with increasing β. In addition, aside from the 3D diffusion models, which provided the poorest agreement with Equation (5) due to the small R^2 values of less than 0.90, the power law, contacting sphere, and contacting cylinder models also yielded smaller values of R^2 at each heating rate considered compared to all models involving $G(X) = [-\ln(1 - X)]^{\alpha}$ for the α values of 1/4, 1/3, 1/2, and 1. Considering these factors,

the first-order Mampel model, also denoted as the 1D Avrami–Erofeev model ($\alpha = 1$), and the 2D ($\alpha = 1/2$), 3D ($\alpha = 1/3$), and 4D ($\alpha = 1/4$) Avrami–Erofeev models exhibited the best linear correlation between $\ln[G(X)]$ and $1000/T$, indicating that these models may potentially represent accurate depictions of the steam gasification reaction of char.

Table 4. Linear coefficient of determination R^2 values obtained with respect to $\ln[G(X)]$ and $1000/T$ using Equation (5) for $0.2 < X \leq 0.8$ at various heating rates β ($K \cdot min^{-1}$) and integral functions $G(X)$.

	Reaction Model	$G(X)$	β = 4	β = 8	β = 12	β = 16	β = 20
1	Power law	$X^{1/4}$	0.992	0.973	0.972	0.961	0.964
2	Power law	$X^{1/3}$	0.995	0.981	0.980	0.971	0.973
3	Power law	$X^{1/2}$	0.990	0.969	0.968	0.957	0.960
4	Power law	$X^{3/2}$	0.968	0.931	0.929	0.912	0.918
5	Mampel (first order)	$-\ln(1-X)$	0.998	0.993	0.992	0.986	0.987
6	Avrami–Erofeev	$[-\ln(1-X)]^{1/2}$	0.998	0.993	0.992	0.986	0.987
7	Avrami–Erofeev	$[-\ln(1-X)]^{1/3}$	0.998	0.993	0.992	0.986	0.987
8	Avrami–Erofeev	$[-\ln(1-X)]^{1/4}$	0.998	0.993	0.992	0.986	0.987
9	Contracting sphere	$1-(1-X)^{1/3}$	0.995	0.981	0.980	0.971	0.973
10	Contracting cylinder	$1-(1-X)^{1/2}$	0.992	0.973	0.972	0.961	0.964
11	One-dimensional diffusion	X^2	0.995	0.981	0.980	0.971	0.973
12	Two-dimensional diffusion	$(1-X)\ln(1-X)+X$	0.992	0.973	0.972	0.961	0.964
13	Three-dimensional diffusion	$1-(1-X)^{1/3}$	0.899	0.868	0.865	0.843	0.851
14	Three-dimensional diffusion	$1-2/3X-(1-X)^{3/2}$	0.864	0.794	0.791	0.764	0.774

The plots and fitted lines obtained from the TGA data in Figure 1 at the carbon conversion ratios X in the range of 0.2–0.8 are presented in Figure 3 for the 1D, 2D, 3D, and 4D Avrami–Erofeev models. In addition, the E_a values obtained from the fitting results corresponding to each heating rate and the E_{ave} values for each model are listed in Table 5, and the table also includes $E_{Starink}$ and the differences between $E_{Starink}$ and the E_{ave} values obtained using the kinetic models. The results in Table 5 indicate that the 3D Avrami–Erofeev model provides the best agreement with $E_{Starink}$. Hence, the 3D Avrami–Erofeev model was selected as the best kinetic model for describing the steam gasification of char in the subsequent investigation.

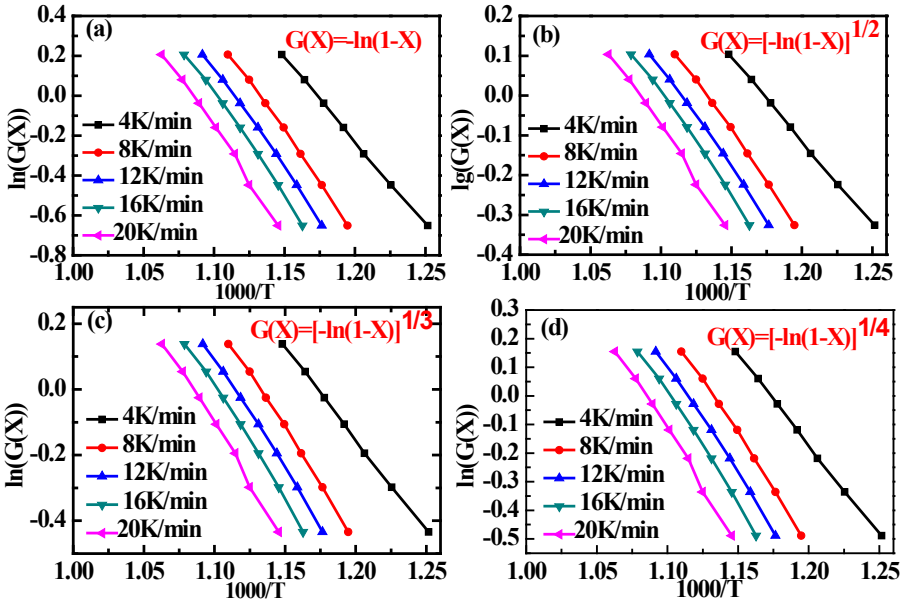


Figure 3. Plots of Equation (5) with $G(X)$ given by the different kinetic models in the form $[-\ln(1-X)]^{\alpha}$ for X values in the range of 0.2–0.8: (**a**) 1D Avrami–Erofeev model ($\alpha = 1$); (**b**) 2D Avrami–Erofeev model ($\alpha = 1/2$); (**c**) 3D Avrami–Erofeev model ($\alpha = 1/3$); (**d**) 4D Avrami–Erofeev model ($\alpha = 1/4$).

Table 5. Activation energies E_a and average E_a values E_{ave} of the steam gasification reaction of char obtained using the various Avrami–Erofeev models at different heating rates β (K·min^{-1}). The E_{ave} value obtained using the Starink method is also given as $E_{Starink}$.

Kinetic Model	E_a (KJ.mol^{-1})					E_{ave}	$E_{Starink}$	$E_{ave} - E_{Starink}$
	β = 4	β = 8	β = 12	β = 16	β = 20			
1D Avrami–Erofeev	72.39	92.91	92.28	95.30	96.46	89.87	135.31	45.44
2D Avrami–Erofeev	96.52	123.88	123.05	127.06	128.61	119.82		15.49
3D Avrami–Erofeev	134.65	133.92	134.79	137.49	139.22	136.01		0.70
4D Avrami–Erofeev	181.19	185.82	184.57	190.60	192.91	187.02		51.71

The value of the pre-exponential factor A was determined for the fitted line in Figure 3c, as obtained under each heating rate, based on the discussion presented in Section 2.3.3. The results indicate that the value of A increased with increasing β, which further demonstrates that the kinetic parameters correlated with the heating rates. This issue is discussed further in the following subsection.

3.4. Application and Analysis

The E_a values obtained by the FWO, KAS, and Starink methods from the TGA results of the char samples derived from the NX, XJ, and NM coal sources (i.e., NX char, XJ char, and NM char) are presented in Figure 4 as a function of X. As observed previously, the E_a values increased with increasing X for all the char samples. The fact that the energetic feasibility of the steam gasification reaction decreased (i.e., E_a increases) with increasing X can be explained by the decreasing availability of active components as the degree of the carbon conversion increased. In addition, the minerals in the char act as a barrier for the diffusion of gaseous components, and the ash layer becomes thicker with increasing X, leading to enhanced gas diffusion resistance and increasing E_a values.

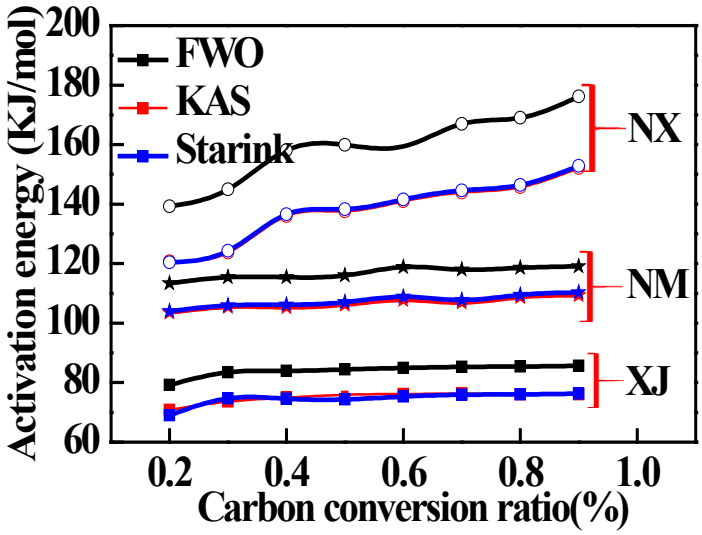


Figure 4. Activation energy E_a values obtained using the FWO, KAS, and Starink methods as a function of X from the TGA results of the char samples derived from the NX, XJ, and NM coal sources (i.e., NX char, XJ char, and NM char).

Once again, we note that the E_a values obtained using the FWO method are somewhat greater than those obtained using the KAS and Starink methods, and that the KAS and Starink methods yield very similar values of E_a, which range from approximately 115–153 KJ.mol^{-1} for the NX char, 70–78 KJ.mol^{-1} for the XJ char, and 103–110 KJ.mol^{-1} for the NM char. Accordingly, the values of E_a obtained for these coal chars decreases in the order of NX char > NM char > XJ char.

The ranges of E_a obtained using the KAS and Starink methods can be compared with the values reported for steam gasification char reactions in the literature, such as E_a = 255 KJ.mol^{-1} for chars derived from low-rank Samhwa coal [24], 105.48–169.10 KJ.mol^{-1} for chars derived from Shenmu Chinese bituminous coal [25], and 282 KJ.mol^{-1} for chars derived from Australian bituminous coal [26,27]. We note that the resulting E_a values obtained here are not in good agreement with these previously reported findings. This can be attributed to variations in the experimental char gasification conditions, which can be affected by many factors, such as the parent coal properties [28], charring conditions [24], and mineral catalytic effects [22].

The values of the pre-exponential factors A were determined for the NX, NM, and XJ chars based on the discussion presented in Section 2.3.3, and the results are presented in Figure 5. Interestingly, the values of A obtained for these coal chars decrease in the same order, i.e., NX char > NM char > XJ char, as that obtained for E_a above. As discussed above, in regard to the NX char sample, the results indicate that the value of A increased with increasing β for all the char samples. This phenomenon is consistent with the results of previous findings and is probably due to the high heating rates applied during the char gasification reactions [29–32]. However, this effect can be limited by the heat and mass transfer. Limitations in the heat transfer can delay the sample heating process, and, thus, the internal temperature of the char particles is always less than the ambient temperature. However, the obtained data were quite similar across gradually increases in the temperature. These results essentially demonstrate that the effects of the heat and mass transfer on the reaction are less significant than those on the TGA.

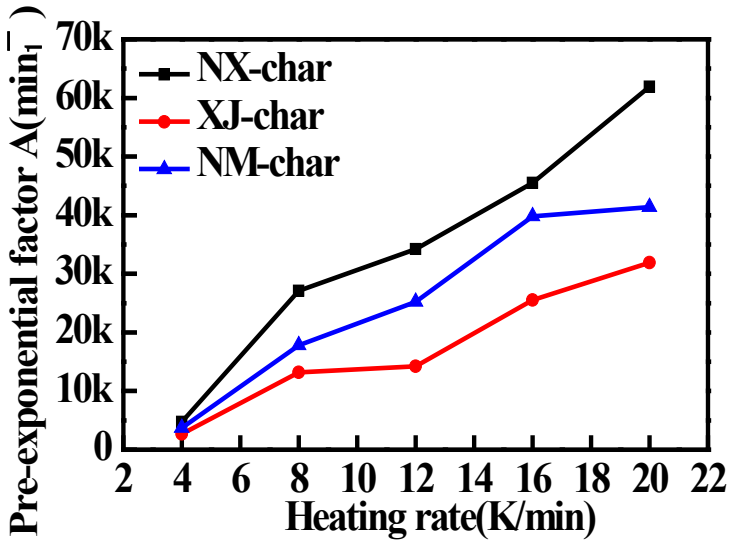


Figure 5. Pre-exponential factors A obtained for the chars derived from the NX, XJ, and NM coal sources as a function of the heating rate.

4. Conclusions

This study addressed the lack of development of the methods for assessing the fitness of kinetic models in representing the important steam gasification reaction of char based on comparisons with kinetic parameters obtained using isoconversional methods. To this end, we conducted a series of steam-assisted char gasification tests using TGA and DTG at five different heating rates. We determined the values of E_a based on the FWO, KAS, and Starink isoconversional methods with different values of X for the NX char sample. Then, we evaluated the degree of fit of a wide variety of kinetic models with the experimental results and compared the average values of E_a obtained using these models with the optimal value obtained using the isoconversional methods. Finally, the reliability of the proposed approach for evaluating the applicability of a given kinetic model to the steam gasification

reaction of char was tested by comparing the results obtained for char samples derived from three different bituminous coal sources. The results yielded the following conclusions:

- The weight loss of the char samples in the steam atmosphere was relatively similar at different heating rates, while the value of X increased with the increasing heating rate.
- The FWO method provided somewhat greater values of E_a than the KAS and Starink methods, while the latter two methods provided consistent E_a values for all the values of X. The average value of E_a obtained by the Starink method ($E_{Starink}$) was deemed optimal.
- The 3D Avrami–Erofeev model provided the best fit with the data, while the 3D Avrami–Erofeev model yielded a value of E_{ave} closest to $E_{Starink}$. The two values differed by only 0.70 KJ.mol^{-1}.
- The values of E_a obtained from the fitted 3D Avrami–Erofeev model for chars derived from the three coal sources decreased in the order of NX char (115–153 KJ.mol^{-1}) > NM char (103–110 KJ.mol^{-1}) > XJ char (70–78 KJ.mol^{-1}). The pre-exponential factor A followed an order of decreasing values consistent with that obtained for E_a.

Supplementary Materials: The following supporting information can be downloaded at: https://www.mdpi.com/article/10.3390/atmos13091480/s1, Table S1. Inorganic constituents mass fraction in coal; Table S2. the heavy metal content of initial coal samples;Figure S1. Coal samples were collected from the Ningdong (NX), Shenxi (SX), and Xinjiang (XJ) coalfields in western China; Figure S2. XRD of the Ningdong (NX), Shenxi (SX), and Xinjiang (XJ) coal.; Figure S3. SEM-EDS of the Ningdong (NX), Shenxi (SX), and Xinjiang (XJ) coal.

Author Contributions: M.A. designed and carried out the quality control, and wrote the manuscript, Q.G. helped with the analyses. Methodology and validation. All authors have read and agreed to the published version of the manuscript.

Funding: This work was supported financially by the Fundamental Research Funds for the Central Universities (Grant No. 2021QN1044), the Natural Science Foundation Project of Ningxia (Grant No. 2022AC03764), State Key Laboratory of High-efficiency Utilization of Coal and Green Chemical Engineering (Grant No.2021-K06). The key R&D projects of Ningxia (Talent special) (Grant No.2021BEB04083).

Institutional Review Board Statement: Not applicable.

Informed Consent Statement: Not applicable.

Data Availability Statement: The data presented in this study are available upon request from the corresponding author.

Acknowledgments: The authors are appreciative for the reviewers' helpful comments and suggestions, which have helped to improve the presentation.

Conflicts of Interest: The authors declare no conflict of interest.

References

1. Brown, M.E.; Maciejewski, M.; Vyazovkin, S.; Nomen, R.; Sempere, J.; Burnham, A.; Opfermann, J.; Strey, R.; Anderson, H.L.; Kemmler, A. Computational aspects of kinetic analysis.: Part A: The ICTAC kinetics project-data, methods and results. *Thermochim. Acta* **2000**, *355*, 125–143. [CrossRef]
2. Kök, M.V. Recent developments in the application of thermal analysis techniques in fossil fuels. *J. Therm. Anal. Calorim.* **2008**, *91*, 763–773. [CrossRef]
3. Vyazovkin, S. Computational aspects of kinetic analysis.: Part C. The ICTAC Kinetics Project—The light at the end of the tunnel. *Thermochim. Acta* **2000**, *355*, 155–163. [CrossRef]
4. Wang, F.; Zeng, X.; Wang, Y.; Su, H.; Yu, J.; Xu, G. Non-isothermal coal char gasification with CO_2 in a micro fluidized bed reaction analyzer and a thermogravimetric analyzer. *Fuel* **2016**, *164*, 403–409. [CrossRef]
5. Ashraf, A.; Sattar, H.; Munir, S. A comparative applicability study of model-fitting and model-free kinetic analysis approaches to non-isothermal pyrolysis of coal and agricultural residues. *Fuel* **2019**, *240*, 326–333. [CrossRef]
6. Liu, Y.; Fu, P.; Bie, K.; Xu, T.; Ahsan, M. Non-isothermal kinetics of coal char oxyfuel combustion by isothermal model-fitting method. *Energy Rep.* **2022**, *8*, 2062–2071. [CrossRef]
7. Yang, S.; Ding, J.; Zhang, X.; Ye, S.; Guo, Z.; Chen, W. Fusion method of model-free and model-fitting for complex reactions in accelerating rate calorimetry. *Thermochim. Acta* **2022**, *712*, 179212. [CrossRef]

8. Mahmood, H.; Shakeel, A.; Abdullah, A.; Khan, M.; Moniruzzaman, M. A Comparative Study on Suitability of Model-Free and Model-Fitting Kinetic Methods to Non-Isothermal Degradation of Lignocellulosic Materials. *Polymers* **2021**, *13*, 2504. [CrossRef]
9. Gomez, A.; Mahinpey, N. A new method to calculate kinetic parameters independent of the kinetic model: Insights on CO_2 and steam gasification. *Chem. Eng. Res. Des.* **2015**, *95*, 346–357. [CrossRef]
10. Mahinpey, N.; Gomez, A. Review of gasification fundamentals and new findings: Reactors, feedstock, and kinetic studies. *Chem. Eng. Sci.* **2016**, *148*, 14–31. [CrossRef]
11. Jain, A.A.; Mehra, A.; Ranade, V.V. Processing of TGA data: Analysis of isoconversional and model fitting methods. *Fuel* **2016**, *165*, 490–498. [CrossRef]
12. Czerski, G.; Zubek, K.; Grzywacz, P.; Porada, S. Effect of Char Preparation Conditions on Gasification in a Carbon Dioxide Atmosphere. *Energy Fuels* **2016**, *31*, 815–823. [CrossRef]
13. Sebakhy, K.O.; Vitale, G.; Hassan, A.; Pereira-Almao, P. New Insights into the Kinetics of Structural Transformation and Hydrogenation Activity of Nano-crystalline Molybdenum Carbide. *Catal. Lett.* **2018**, *148*, 904–923. [CrossRef]
14. Byambajav, E.; Hachiyama, Y.; Kudo, S.; Norinaga, K.; Hayashi, J. Kinetics and Mechanism of CO_2 Gasification of Chars from 11 Mongolian Lignites. *Energy Fuels* **2015**, *30*, 1636–1646. [CrossRef]
15. Korotkikh, A.G.; Slyusarskiy, K.V. Kinetic study of coals gasification into carbon dioxide atmosphere. *MATEC Web Conf.* **2015**, *23*, 1020. [CrossRef]
16. Gomez, A.; Mahinpey, N. Kinetic study of coal steam and CO_2 gasification: A new method to reduce interparticle diffusion. *Fuel* **2015**, *148*, 160–167. [CrossRef]
17. Gomez, A.; Silbermann, R.; Mahinpey, N. A comprehensive experimental procedure for CO_2 coal gasification: Is there really a maximum reaction rate? *Appl. Energy* **2014**, *124*, 73–81. [CrossRef]
18. Yang, Z.; Gao, M.; Wang, Y.; Bai, Y.; Li, F. Identification for the behavior of maximum reaction rate during the initial stage of coal char gasification. *J. Therm. Anal. Calorim.* **2017**, *128*, 1183–1194. [CrossRef]
19. Vyazovkin, S.; Burnham, A.K.; Criado, J.M.; Pérez-Maqueda, L.A.; Popescu, C.; Sbirrazzuoli, N. ICTAC Kinetics Committee recommendations for performing kinetic computations on thermal analysis data. *Thermochim. Acta* **2011**, *520*, 1–19. [CrossRef]
20. Doyle, C.D. Estimating isothermal life from thermogravimetric data. *J. Appl. Polym. Sci.* **1962**, *6*, 639–642. [CrossRef]
21. Liu, H.; Zhu, H.; Kaneko, M.; Kato, S.; Kojima, T. High-Temperature Gasification Reactivity with Steam of Coal Chars Derived under Various Pyrolysis Conditions in a Fluidized Bed. *Energy Fuels* **2010**, *24*, 68–75. [CrossRef]
22. Zhang, Y.; Hara, S.; Kajitani, S.; Ashizawa, M. Modeling of catalytic gasification kinetics of coal char and carbon. *Fuel* **2010**, *89*, 152–157. [CrossRef]
23. Wang, Y.L.; Zhu, S.H.; Gao, M.Q.; Yang, Z.R.; Yan, L.J.; Bai, Y.H.; Li, F. A study of char gasification in H_2O and CO_2 mixtures: Role of inherent minerals in the coal. *Fuel Process. Technol.* **2015**, *141*, 9–15. [CrossRef]
24. Dai, P.; Dennis, J.S.; Scott, S.A. Using an experimentally-determined model of the evolution of pore structure for the gasification of chars by CO_2. *Fuel* **2016**, *171*, 29–43. [CrossRef]
25. Jayaraman, K.; Gokalp, I.; Bonifaci, E.; Merlo, N. Kinetics of steam and CO_2 gasification of high ash coal–char produced under various heating rates. *Fuel* **2015**, *154*, 370–379. [CrossRef]
26. Fan, D.; Zhu, Z.; Na, Y.; Lu, Q. Thermogravimetric analysis of gasification reactivity of coal chars with steam and CO_2 at moderate temperatures. *J. Therm. Anal. Calorim.* **2013**, *113*, 599–607. [CrossRef]
27. Everson, R.C.; Okolo, G.N.; Neomagus, H.W.J.P.; Dos Santos, J. X-ray diffraction parameters and reaction rate modeling for gasification and combustion of chars derived from inertinite-rich coals. *Fuel* **2013**, *109*, 148–156. [CrossRef]
28. Everson, R.C.; Neomagus, H.W.J.P.; Kaitano, R.; Falcon, R.; du Cann, V.M. Properties of high ash coal-char particles derived from inertinite-rich coal: II. Gasification kinetics with carbon dioxide. *Fuel* **2008**, *87*, 3403–3408. [CrossRef]
29. Fermoso, J.; Gil, M.V.; García, S.; Pevida, C.; Pis, J.J.; Rubiera, F. Kinetic Parameters and Reactivity for the Steam Gasification of Coal Chars Obtained under Different Pyrolysis Temperatures and Pressures. *Energy Fuels* **2011**, *25*, 3574–3580. [CrossRef]
30. Liu, Z.; Wang, Q.; Zou, Z.; Tan, G. Arrhenius parameters determination in non-isothermal conditions for the uncatalyzed gasification of carbon by carbon dioxide. *Thermochim. Acta* **2011**, *512*, 1–4. [CrossRef]
31. Ding, H.; Jiang, Y.; Chen, Y.F.; Li, W.H. Experimental study on gasification kinetics of Lu'an coal char with steam by non-isothermal thermogravimetry. *J. China Coal Soc.* **2010**, *35*, 666–669.
32. Edreis, E.M.A.; Luo, G.; Yao, H. Investigations of the structure and thermal kinetic analysis of sugarcane bagasse char during non-isothermal CO_2 gasification. *J. Anal. Appl. Pyrol.* **2014**, *107*, 107–115. [CrossRef]